Available online at www.sciencedirect.com
ScienceDirect
Trans. Nonferrous Met. Soc. China 31(2021) 1381−1396
Transactions of Nonferrous Metals Society of China
www.tnmsc.cn

Molecular dynamics simulation on mechanisms of plastic anisotropy in nanotwinned polycrystalline copper with {111} texture during tensile deformation

Yan-qiu ZHANG, Shu-yong JIANG

College of Mechanical and Electrical Engineering, Harbin Engineering University, Harbin 150001, China

Received 22 April 2020; accepted 28 December 2020

Abstract: Based on molecular dynamics (MD) simulation, the mechanisms of plastic anisotropy in nanotwinned polycrystalline copper with {111} texture during tensile deformation were systematically studied from the aspects of Schmid factor of the dominant slip system and the dislocation mechanism. The results show that the Schmid factor of dominated slip system is altered by changing the inclining angle of the twin boundaries (TBs), while the yield stress or flow stress does not strictly follow the Schmid law. There exist hard and soft orientations involving different dislocation mechanisms during the tensile deformation. The strengthening mechanism of hard orientation lies in the fact that there exist interactions between the dislocations and the TBs during plastic deformation, which leads to the dislocation blocking and reactions. The softening mechanism of soft orientation lies in the fact that there is no interaction between the dislocations and the TBs because only the slip systems parallel to the TBs are activated and the dislocations slip on the planes parallel to the TBs. It is concluded that the plastic anisotropy in the nanotwinned polycrystalline copper with {111} texture is aroused by the combination effect of the Schmid factor of dominated slip system and the dislocation mechanism.

Key words: mechanical property; dislocations; molecular dynamics; plastic anisotropy; nanotwins

1 Introduction

Ultrafine-grained polycrystalline copper with thin nanotwins embedded in individual grains has attracted much attention since it was synthesized in the last decade. The strength of the nanotwinned copper is 7−10 times higher than that of conventional coarse-grained polycrystalline copper. Meanwhile, the nanotwinned copper also possesses considerable ductility as well as excellent electrical conductivity [1−4]. More interestingly, both the grain size and the twin spacing were found to have a significant influence on the strength of such nanotwinned copper, but their influence is non-monotonous. In other words, the strength first increases with decreasing grain size or twin spacing and it reaches a maximum value at the grain size ranging from 10 to 15 nm or the twin spacing of 15 nm. Then, it decreases with the further decrease of the grain size or the twin spacing [4,5]. The emergence of this class of nanostructured materials opens a way that obtains unprecedented properties by means of adjusting the coherent internal boundaries of materials [6−8]. As a consequence, this kind of unique nanotwinned structure has been intensively investigated over the past ten years. These studies are mainly focused on the mechanisms for the plastic deformation of the nanotwinned copper, and it has been evident that the twin boundary (TB), a special kind of coincidence site lattice boundary, plays a significant role during the plastic deformation of metals [9−15]. On one hand, the twin boundaries (TBs) could act

Corresponding author: Shu-yong JIANG, Tel: +86-13936266338, E-mail: jiangshy@sina.com
DOI: 10.1016/S1003-6326(21)65584-X

as the barriers to the motion of dislocations like conventional grain boundaries (GBs), which enhances the strength of materials [1,7,9]. On the other hand, the TB is also a slip plane, which could take part in the dislocation reactions to improve the ductility of materials [7,8,10−12,16−20]. LU et al [21] concluded that the deformation behavior in nanotwinned copper mainly results from four components, including the Shockley partial dislocations (SPDs) slipping at TBs, the sessile dislocations locked at TBs, the extended stacking faults terminated at TBs and threading dislocations in the matrix or twin lamellae. Among these components, the SPDs at TBs and the threading dislocations within matrix or twin lamellae are mobile dislocations, which contribute to the enhancement of the ductility. However, the extended stacking faults and dislocations locked at TBs are immobile ones, which lead to the work hardening and the ultrahigh strength. In addition, the influence of twin spacing and grain size on the strength has been deeply investigated as well. It has been found that the occurrence of maximum strength in the grain size variation is due to the shift from dislocation-dominated mechanism in coarse-grained materials to GB sliding-dominated mechanism in the nanocrystalline ones [5,22,23]. The emergence of maximum strength in the twin spacing variation is attributed to the transition of deformation mechanism from the occurrence of cross-slip and dissociation in lamellae with large twin spacing to the absence of cross-slip and dissociation in lamellae with small twin spacing [24]. Furthermore, the influence of some other factors, such as the strain rate, the temperature and the grain shape, has been investigated as well [18,25−28]. A newest investigation on a gradient nanotwinned copper with highly tunable structural gradients shows that increasing the structural gradient is able to substantially strengthen the nanotwinned materials [29]. As a consequence, the mechanisms of plastic deformation in the nano-twinned copper are very complicated and deserve further study.

Recently, highly oriented nanotwinned polycrystalline copper has been synthesized [30]. This kind of material usually presents plastic anisotropy because its deformation mechanisms have a strong dependence on the loading orientation relative to the TBs. It has been reported that different mechanical properties were obtained when the highly nanotwinned copper is loaded at different orientations [31−34]. JANG et al [31] studied the deformation mechanisms in single crystalline nanotwinned copper nanopillars by virtue of experiment and atomistic simulation, and they found that the strength of the sample under the loading direction perpendicular to TBs is higher than that of the sample inclining 18° to the TBs. ZHAO et al [32] investigated the deformation twinning as well as dislocation evolution in single crystalline nanotwinned copper by means of molecular dynamics (MD) simulation, and they found that deformation twins are induced along one primary twinning system when the angle between the loading direction and the TBs is close to 75°, while symmetric twinning in both matrix and twinned lamellae is formed when the angle between the loading direction and the TBs is close to 90°. However, both of the above studies were related to the nanotwinned copper without GBs. YOU et al [33] investigated plastic anisotropy and associated deformation mechanisms in columnar-nanotwinned copper with {111} texture by means of experiment, crystal plastic finite element simulation and MD simulation, and they found that the operated deformation mechanism is able to be altered among three dislocation modes by changing the angle between the loading direction and the TBs. HUANG et al [34] studied the influence of TB tilt angle on the strength of columnar-nanotwinned copper by virtue of MD simulation. However, both of the above studies simplified the MD simulation models as the pure columnar grains without GBs in the dimension parallel to the direction of the columnar grain length during their MD simulations. Indeed, the nanotwinned polycrystalline copper obtained from experiments is usually composed of columnar grains with GBs in all the three dimensions [30,35]. It is well known that the GBs are the main initiation sites of dislocations during the plastic deformation of metal materials [36−38]. If the GBs in the dimension parallel to the direction of the columnar grain length are neglected, the dislocation emission mechanism will be altered during the simulation, which is incapable of reflecting the experimental results very well. As a consequence, the mechanisms of plastic anisotropy

in the nanotwinned polycrystalline copper with {111} texture and with GBs in three dimensions were investigated by means of MD simulation in the present study.

2 Modeling and method

In the present study, five simulation models with {111} texture were constructed for the purpose of investigating the mechanisms of plastic anisotropy in nanotwinned polycrystalline copper by means of Voronoi construction method [39], as shown in Fig. 1. Even if the grain shape in these models is not columnar, the GB conditions agree with the ones in the experiments, which is more important in investigating the deformation mechanisms. Each simulation model consists of eight grains with nanotwins, where the twinning plane is (111). All of the five models were constructed with the same size of 30 nm × 30 nm × 30 nm and the same copper atoms of 2285899. Meanwhile, all of the models are {111}-textured and they possess the same grain shape, grain size and twin spacing in each corresponding grain. According to Ref. [5], the nanocrystalline copper exhibits the maximum strength at the grain size ranging from 10 to 15 nm, so the mean grain size of 15 nm was set in the present study. Based on Ref. [4], the nanotwinned copper presents the maximum strength at the twin spacing of 1.25 nm when the grain size is 10 nm, while it exhibits the maximum strength at the twin spacing of 2.08 nm when the grain size is 20 nm. Therefore, the maximum strength should occur at the twin spacing ranging from 1.25 to 2.08 nm when the mean grain size is 15 nm. As a consequence, the twin spacing of 1.878 nm, which is equal to the length of three unit cells of copper in ⟨111⟩ direction ($\sqrt{3}a\times3=1.878$ nm, where a=0.3615 nm is the lattice constant of copper) was selected in the present study. The only difference among the five simulation models lies in the TB inclining angle with respect to the z direction, where the angles of them were set to be 0°, 30°, 45°, 60° and 90°, respectively. The embedded-atom method (EAM) potential developed by MISHIN et al [40] was used to calculate the atomic interactions among copper atoms. This potential has been proven to be able to accurately reproduce the properties of copper [24,33,41]. Periodic boundary condition was imposed on all the three dimensions for the purpose of modeling bulk materials. All of the models were firstly minimized at 300 K by virtue of conjugate gradient method and then they were equilibrated for 50 ps at the same temperature, during which the isobaric isothermal (NPT) ensemble was used. Subsequently, the models were heated to 600 K at the heating rate of 5 K/ps and then were annealed at this temperature for 50 ps before being cooled to 300 K at the cooling rate of 5 K/ps. Finally, at a constant temperature of 300 K, all the models were loaded to a uniaxial tensile strain with a constant strain rate of 5×10^8 s^{-1} along z direction, while the NPT ensemble with zero stress was imposed on the

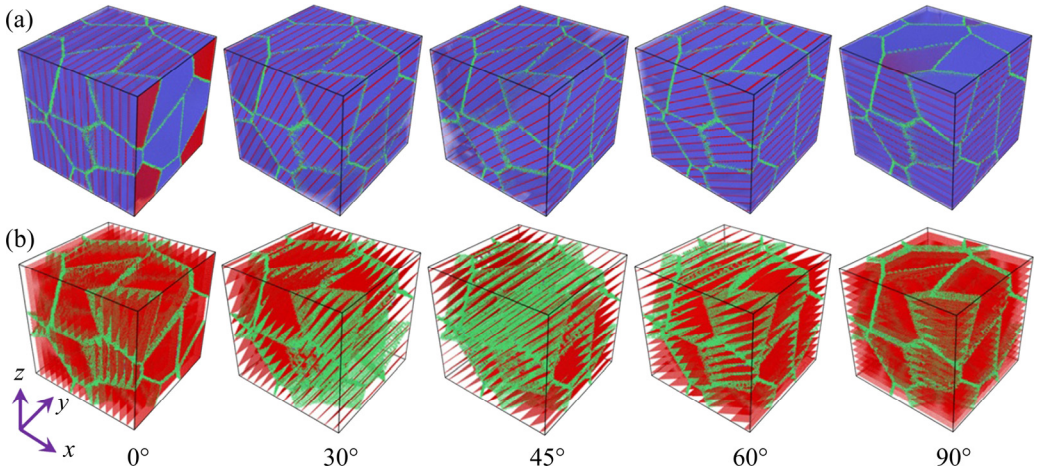

Fig. 1 Simulation models with various TB inclining angles: (a) Atomic configurations; (b) Configurations with face-centered cubic (FCC) structure concealed (The atoms are coloured according to the common neighbour analysis (CNA), where the atoms coloured in blue represent the FCC structure, the atoms coloured in green stand for the grain boundaries, and the atoms coloured in red denote the hexagonal close-packed (HCP) structure)

other two directions so that the models are able to freely shrink or expand during the deformation. As a consequence, the five simulation models can be named after the angles between loading direction and the TBs, which are 0°, 30°, 45°, 60° and 90°, respectively.

The MD simulation was performed using parallel MD package LAMMPS established by PLIMPTON [42]. During the simulation, a volume-averaged stress proposed by ZHANG and GHOSH [43] was used to study the global mechanical behaviors of the models, as expressed in the following equation:

$$\sigma_{ij}=\frac{1}{V_{\text{box}}}\left[\sum_{k}^{N}(m^k v_i^k v_j^k)+\sum_{k}^{N}(r_i^k f_j^k)\right] \quad (1)$$

where i and j represent two axes in Cartesian coordinate, and they range from 1 to 3, respectively, k is used to identify an atom in a system consisting of N atoms, V_{box} is the volume of the simulation box, v_i^k is component of velocity vector for atom k, r_i^k is component of position vector for atom k, m^k is atomic mass of atom k, and f_j^k denotes the force imposing on atom k and it results from the pairwise interaction.

The OVITO scientific software package was used in order to visualize the simulated configurations. For the purpose of visualizing the defects such as dislocations, stacking faults, twin boundaries and grain boundaries, atoms were expressed by various colours according to the local crystalline order by means of common neighbour analysis (CNA). In this study, the atoms coloured in blue represent the face-centered cubic (FCC) structure and the atoms coloured in green stand for grain boundaries, dislocation cores and other defects. However, the atoms coloured in red denote the hexagonal close-packed (HCP) structure, where one layer of red atoms represent twin boundary and two layers of red atoms adjacent to or separated by a layer of FCC atoms stand for stacking faults. Moreover, the dislocation extraction algorithm (DXA) proposed by STUKOWSKI [44] was adopted so as to characterize the dislocations. This algorithm is able to extract the dislocation lines and identify the corresponding Burgers vectors, which provide detailed information for the dislocation analysis.

3 Results

3.1 Anisotropic behaviors of plastic deformation

Figure 2 shows the tensile stress–strain curves obtained from MD simulation. On these curves, the first peaks correspond to the yield stresses where dislocations are initially nucleated in the annealed models. When enough dislocations which can accommodate the steady plastic deformation are accumulated, the stresses of all the models drop to a lower level, which is defined as flow stress. From Fig. 2, it is observed that obviously plastic anisotropy appears during the tensile deformation of nanotwinned polycrystalline copper with {111} texture, which can be clearly observed in the yield stresses of the curves. In the case of 90°, the yield stress σ_{90} reaches a high value of 5.5 GPa, which is much higher than that of other angles, whereas in the case of 45°, the yield stress σ_{45} presents the lowest value of 1.9 GPa. However, when the angle between the loading direction and the TBs is 0°, the value of yield stress σ_0 is between that of σ_{90} and σ_{45}. In addition, the flow stresses of the above three cases follow the above law as well. This law is in accordance with the results obtained in the nanotwinned polycrystalline copper with {111} texture [33]. In the cases of 30° and 60°, the value of yield stress σ_{30} of 30° model is between those of 0° and 45°, while the value of 60° model is between those of 45° and 90°. However, the flow stresses of these two cases do not present above characteristics.

3.2 Microstructural characteristics

Figure 3 illustrates the atomic configurations

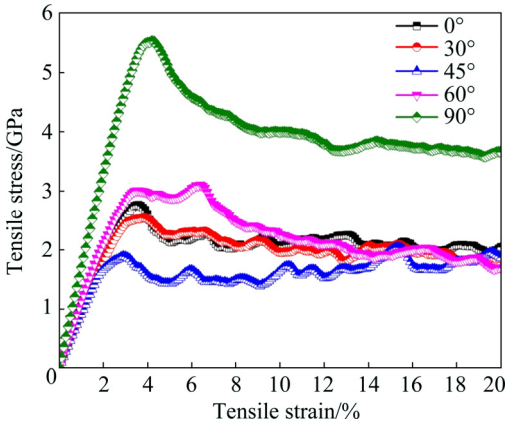

Fig. 2 Tensile stress–strain curves obtained from MD simulation

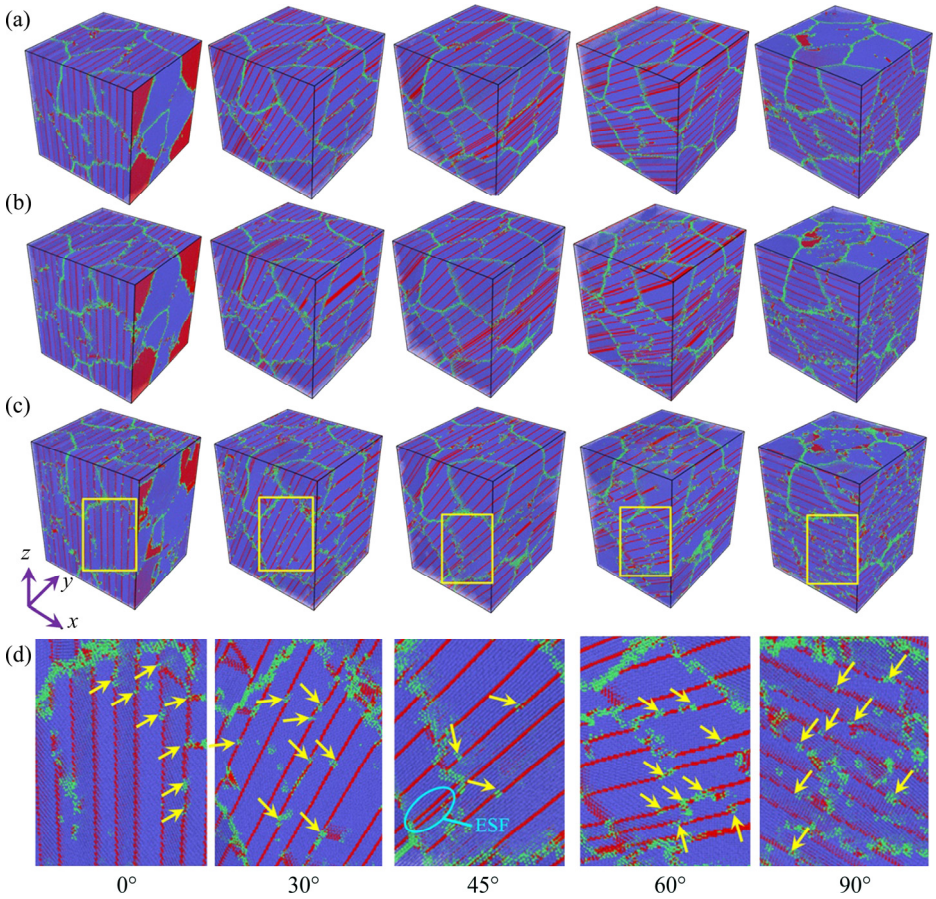

Fig. 3 Atomic configurations of five models subjected to various strains: (a) 5%; (b) 10%; (c) 20%; (d) Magnifications of rectangular regions in (c) (ESF stands for extrinsic stacking fault)

of the five simulation models subjected to various strains. It can be seen that the five models present different slip characteristics during the plastic deformation. In the cases of 0° and 90°, only the dislocations intersecting with TBs can be observed, while only the dislocations parallel to TBs are seen as for 45°. However, both the dislocations intersecting and the ones parallel to TBs are found in the cases of 30° and 60°. These phenomena indicate that the anisotropic behaviors of plastic deformation in nanotwinned polycrystalline copper with {111} texture are closely related to the mechanisms of dislocation nucleation and evolution. In addition, there exist many nanometer-sized steps at the TBs in all of the five models, as shown in positions pointed by the yellow arrows in Fig. 3(d). These steps cause the morphology of coherent TBs to change from flat to rough. In addition, it can be also observed from Fig. 3 that migration of TBs occurs in all of the models, which can be confirmed by the variations of twin spacing during the plastic deformation.

Figure 4 shows the dislocation distributions of the five models at the strain of 20%. It can be noted that SPDs are dominant in all of the five models, and dislocations are mainly distributed between two adjacent TBs. There exists significant difference in the dislocation distribution among various models, and the dislocation density among various grains of the same model is different as well. These phenomena illustrate that the nucleation and evolution of dislocations are influenced by both the loading direction and the grain orientation in the nanotwinned polycrystalline copper with {111} texture. Furthermore, it can be observed from Figs. 4(b, c) that dislocations are mainly propagated along the direction parallel to the TBs, which indicates that the TBs act as the barriers of dislocation motion.

In order to illustrate the above differences, the detailed information for dislocation evolution of three representative models with the inclining degree of 0°, 45° and 90° is captured, as shown in Figs. 5−7. It can be noted from Fig. 5 that in the

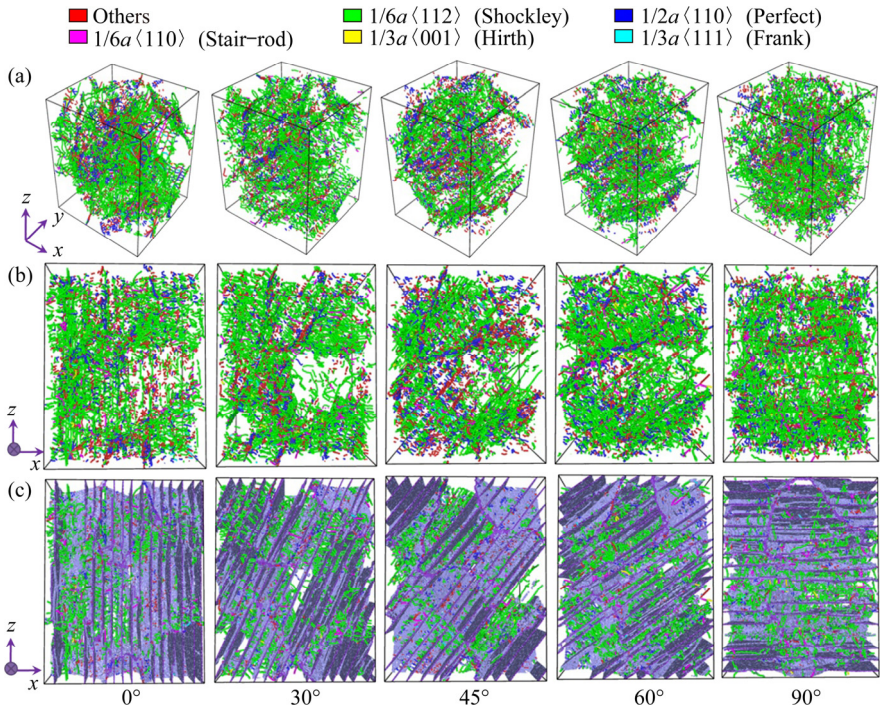

Fig. 4 Dislocation distributions in five models at strain of 20%: (a) Isometric view; (b) *y* view; (c) *y* view with interface mesh added

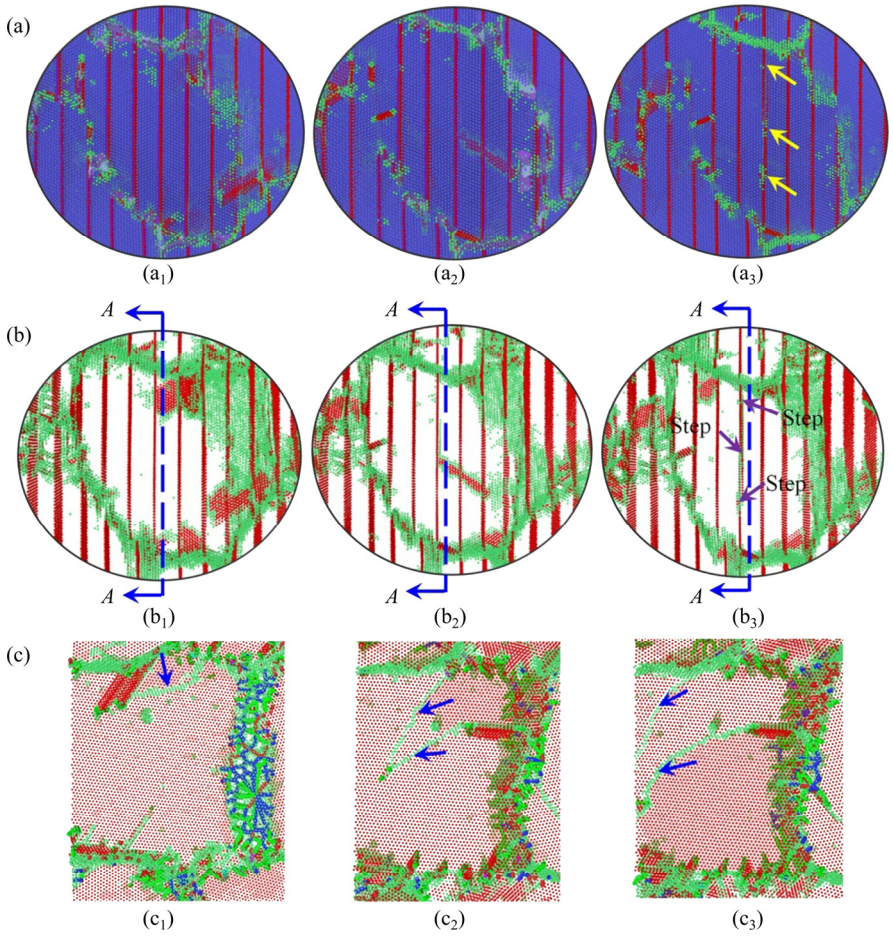

Fig. 5 Detailed information for dislocation evolution in model with inclining degree of 0°: (a) Atomic configurations of interested grain; (b) Atomic configurations in (a) with FCC atoms concealed; (c) *A*−*A* profiles of atomic configurations in (b) with dislocations added (The evolution occurs from left to right (1−3))

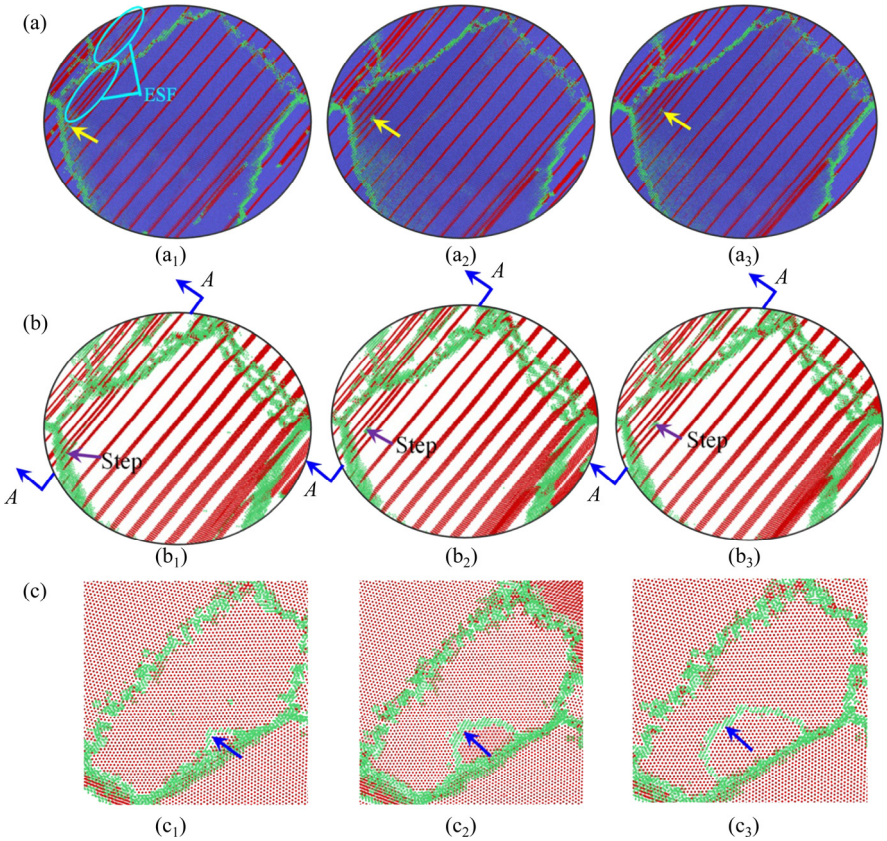

Fig. 6 Detailed information for dislocation evolution in model with inclining degree of 45°: (a) Atomic configurations of interested grain; (b) Atomic configurations in (a) with FCC atoms concealed; (c) *A*−*A* profiles of atomic configurations in (b) with dislocations added (The evolution occurs from left to right (1−3))

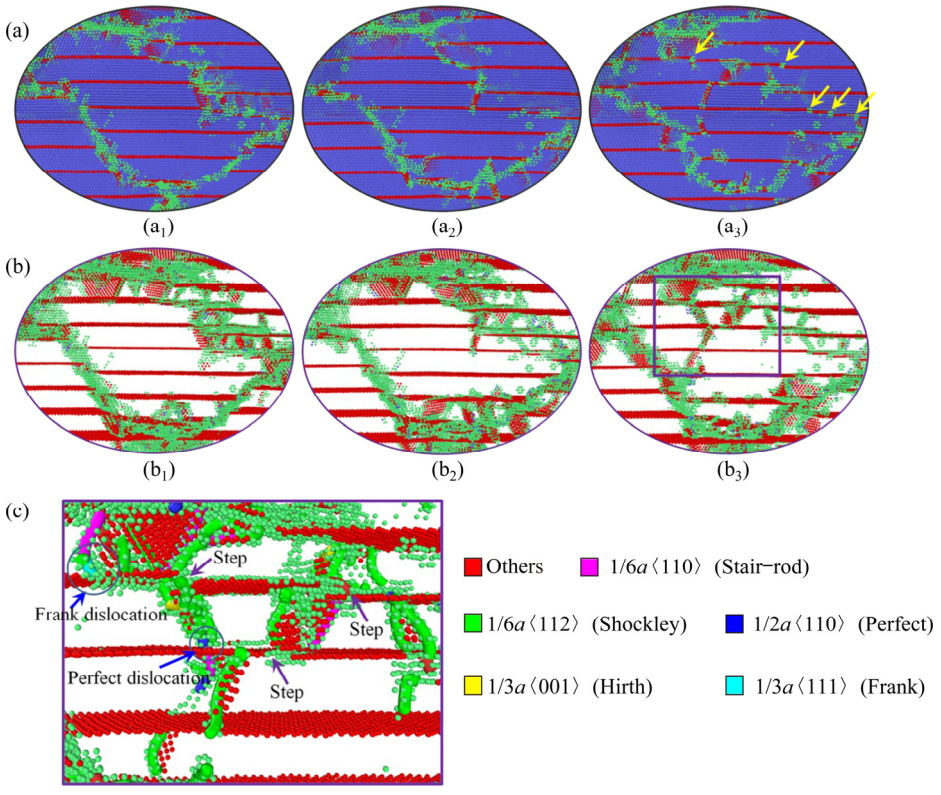

Fig. 7 Detailed information for dislocation evolution in model with inclining degree of 90°: (a) Atomic configurations of interested grain; (b) Atomic configurations in (a) with FCC atoms concealed; (c) Profile of atomic configurations in (b_3) with dislocations added (The evolution in (a) and (b) occurs from left to right (1−3))

case of 0°, the SPDs are initiated from the GBs and they are emitted in the directions inclining a certain angle to the TBs. When these SPDs encounter the TBs, they are impeded by TBs and new SPDs slipping on the TBs are induced, as shown in Fig. 5(c). It is the SPDs slipping on the TBs that form the steps on the TBs, as shown in the positions pointed by the yellow arrows in Fig. 5(a_3) and the ones pointed by purple arrows in Fig. 5(b_3). It can be found from Fig. 6 that in the case of 45°, the SPDs are initiated from GBs as well, but they are emitted and slip along the directions parallel to the TBs, as shown in Fig. 6(c). As a consequence, the steps on the TBs in this case result from the SPDs initiated from the junctions between GBs and TBs. In addition, no SPDs in other directions are observed except the ones parallel to the TBs. It can be observed from Fig. 7 that in the case of 90°, the SPDs are also initiated from the GBs and they are subsequently emitted in the directions inclining a certain degree to the TBs, which resembles the case of 0°. However, a great difference is observed after they encounter the TBs. In this case, a SPD hampered by the TB can be dissociated into two parts, where one part slips along the twin plane while the other part passes through the twin plane and joins in another dislocation emission process, which can be confirmed by Fig. 7(c).

4 Discussion

According to above results, it can be noted that the loading orientation has an important effect on the mechanical properties of nanotwinned polycrystalline copper with {111} texture as well as its deformation mechanisms. In other words, there exists plastic anisotropy during the plastic deformation of nanotwinned polycrystalline copper with {111} texture. In general, the mechanisms of plastic anisotropy are closely related to the activated slip systems of a metal material [45−47]. In order to investigate the mechanisms for the plastic anisotropy, the primary slip systems in three representative models with the inclining angle of 0°, 45° and 90° are illustrated in Fig. 8. In the case of 0°, crystallographic orientations of the two lamellae

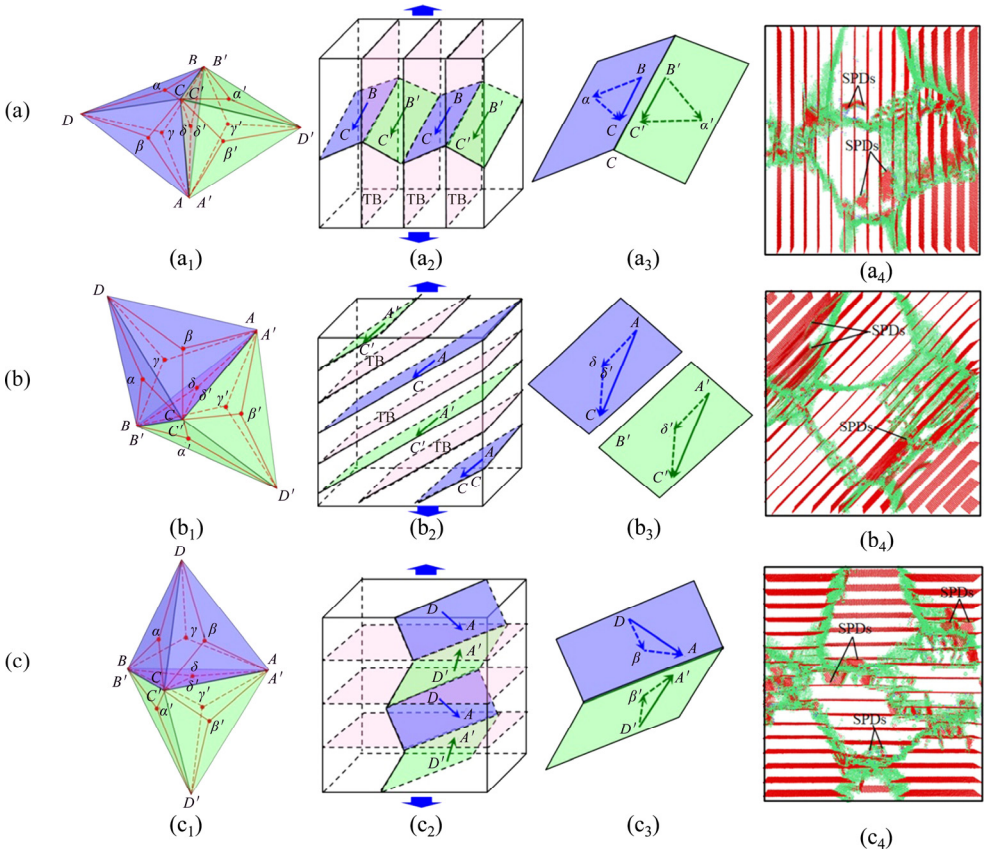

Fig. 8 Primary slip systems in three representative models with inclining angle of 0° (a), 45° (b) and 90° (c): (a_1, b_1, c_1) Double Thompson tetrahedron for twinned FCC structure; (a_2, b_2, c_2) Primary slip systems; (a_3, b_3, c_3) Shockley partial dislocations (SPDs) in primary slip systems; (a_4, b_4, c_4) Simulated results

(matrix lamella and twin lamella) on both sides of a TB are symmetrical about the loading direction, so they possess the same distribution of Schmid factor. As a consequence, the primary slip systems, i.e. the slip systems whose Schmid factor is the highest in matrix or twin lamellae, are those on the slip planes intersecting with TB and simultaneously with the slip directions parallel to TB [48], as depicted in Fig. 8(a). According to the double Thompson tetrahedron in Fig. 8(a), the primary slip systems in the matrix should be one of the three slip vectors ($\overrightarrow{AB}$, $\overrightarrow{BC}$ and $\overrightarrow{CA}$) on the slip plane *ABC*, depending on the angle between the loading direction and the corresponding vector. In the present study, $\overrightarrow{BC}$ is supposed to be the primary slip system of the matrix, and then $\overrightarrow{B'C'}$ should be the primary slip system of the twin. For the purpose of convenience, such slip systems are represented as S1 in the following text. In the case of 45°, the primary slip systems of the two lamellae on both sides of TB possess the slip planes and the slip directions parallel to the TBs, as illustrated in Fig. 8(b). According to the double Thompson tetrahedron in Fig. 8(b), the primary slip systems in the matrix should be one of the three slip vectors ($\overrightarrow{AB}$, $\overrightarrow{BC}$ and $\overrightarrow{CA}$) on the slip plane *ABC*, depending on the angle between the loading direction and the corresponding vector. If the slip vector $\overrightarrow{AC}$ is supposed to be primary slip system in the matrix, and then the slip vector $\overrightarrow{A'C'}$ should be the primary slip system in the twin. For convenience, such slip systems are specified as S2 in the following text. As for the case of 90°, the loading direction is normal to the TBs, so the primary slip systems of the two lamellae on both sides of a TB could be any one on slip planes intersecting with the TBs, as shown in Fig. 8(c). According to the double Thompson tetrahedron in Fig. 8(c), the primary slip systems in the matrix should be any one of the three slip vectors ($\overrightarrow{DA}$, $\overrightarrow{DB}$ and $\overrightarrow{DC}$) because they have the same inclining angles with respect to the loading direction and the slip planes in which they are located also have the same inclining angles with respect to loading direction. As a consequence, such multiple-slip systems are denoted as S3 in the following text. To simplify, only a pair of representative slip systems, i.e. $\overrightarrow{DA}$ on the slip plane *ACD* and $\overrightarrow{D'A'}$ on the slip plane *A'C'D'*, are sketched in Fig. 8(c). All of the above slip systems are represented by the perfect dislocations. Indeed, a perfect dislocation slip in the metal materials is usually realized by the slip of two SPDs. In other words, a perfect dislocation is able to be dissociated into two SPDs, as shown in Figs. 8(a_3, b_3, c_3), which can be confirmed by the corresponding simulated results shown in Figs. 8(a_4, b_4, c_4). As a consequence, SPDs are observed to be dominant during the plastic deformation of all the five models.

Based on the above analysis, it can be noted that the behaviors of plastic anisotropy in nanotwinned polycrystalline copper with {111} texture are affected by the combination of loading orientation and the dominated slip systems. Figure 9 illustrates the distributions of Schmid factor in the operated slip systems of the three representative models. It can be seen that the S2 slip system dominating in the 45° model possesses the highest Schmid factor, while the S3 slip system operating in the 90° model has the lowest values of Schmid factor. The Schmid factor of S1 slip systems dominating in the 0° model is between those of S2 and S3 slip systems and they are closer to those of S2 slip system. This agrees with the laws of tensile stress–strain curves shown in Fig. 2. However, these values of Schmid factor are not inversely proportional to the yield stresses or the flow stresses of the three models. As a consequence, the plastic anisotropy of nanotwinned polycrystalline copper with {111} texture must be influenced by some other factors.

In order to investigate the other factors that influence the behaviors of plastic anisotropy in nanotwinned polycrystalline copper with {111}

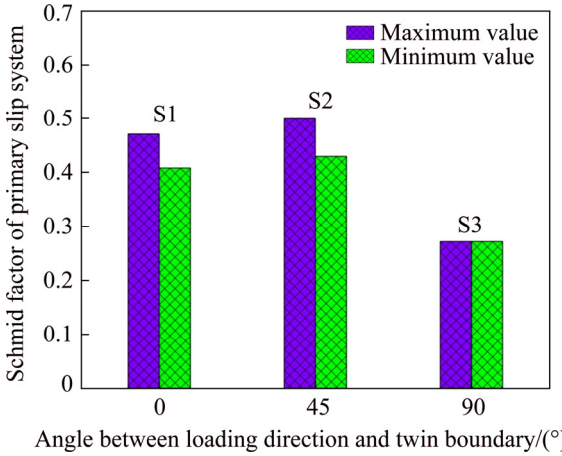

Fig. 9 Distributions of Schmid factor in operated slip systems of three representative models with different inclining angles

texture, schematic illustrations for the dislocation nucleation, evolution and interactions in the three representative models are drawn based on the aforementioned results and analysis. Figure 10(a) gives the schematic illustration for the dislocation nucleation, evolution and interaction in the model with the inclining angle of 0°, where αC is firstly initiated from the GB as a leading partial dislocation and $B\alpha$ is subsequently emitted from the GB as a trailing partial dislocation. It is well known that the slip of a leading partial dislocation can induce an intrinsic stacking fault (ISF) (two adjacent layers of HCP atoms in the configurations, as illustrated in Fig. 11(a)) in its sweeping region, while a trailing partial dislocation behind it is able to eliminate the ISF induced by the leading one [49−51]. As a result, there exists an ISF region between the leading and trailing partial dislocations, as shown in Fig. 10(a_1). This pair of SPDs slip in the matrix and finally encounter the TB, where a perfect dislocation BC is formed and it is blocked at the TB, as shown in Fig. 10(a_2). Similarly, a pair of SPDs including the leading partial dislocation $\alpha'C'$ and the trailing partial dislocation $B'\alpha'$ are emitted from the GB and they slip in the twin, as shown Fig. 10(a_1). Finally, a perfect dislocation $B'C'$ is formed and blocked at the TB when they encounter the TB, as shown Fig. 10(a_2). According to Fig. 3 and Fig. 5, many SPDs slipping on the TB planes have been induced. Because the normal direction of the TB planes in this case is perpendicular to the loading one, the Schmid factor of slip systems on these planes should be zero and no dislocations could be induced under the loading stress in this case. Consequently, the dislocations slipping on the TB planes should be induced by dislocation dissociation rather than the loading stress in the case of 0°. As a result, this phenomenon can be explained as follows. With the increase of density of the blocked dislocations, stress concentration is induced at the sites where the dislocations are blocked, which triggers the dissociation of the perfect dislocations BC or $B'C'$. This dislocation reaction can be expressed as

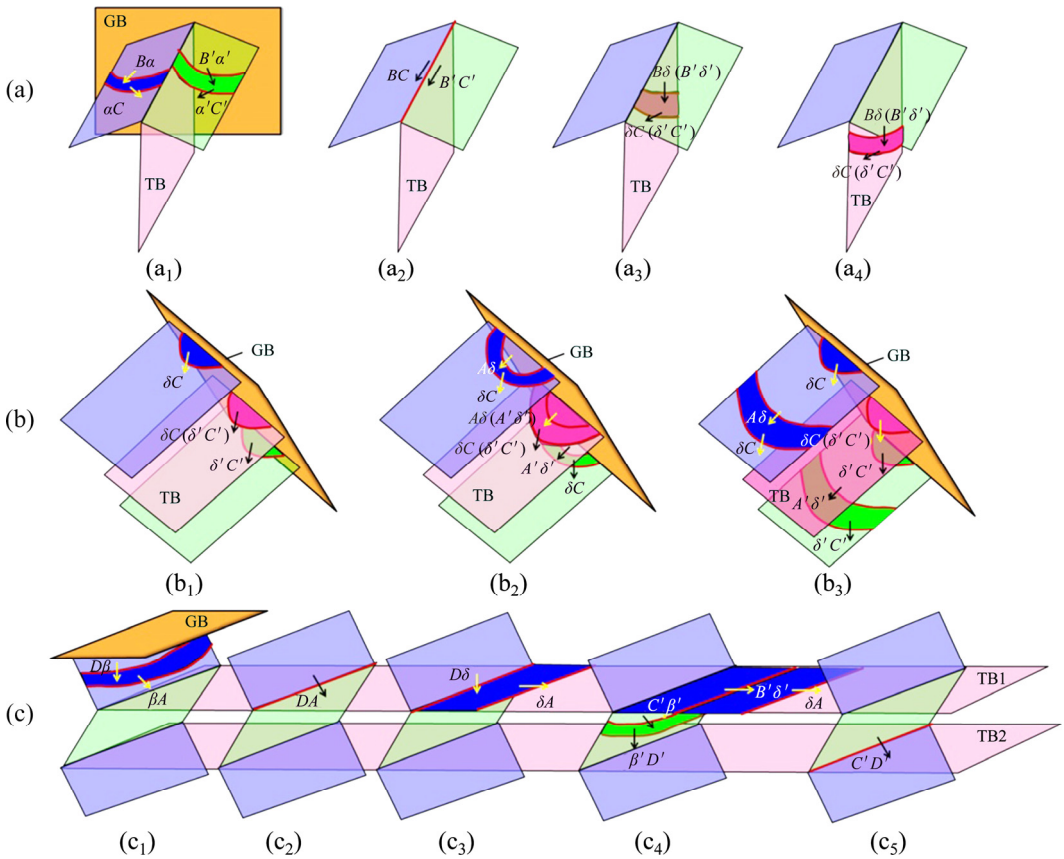

Fig. 10 Schematic illustrations for dislocation nucleation, evolution and interaction in three representative models with inclining angle of 0° (a), 45° (b) and 90° (c) (The evolution in (a), (b) and (c) occurs from left to right of 1−4, 1−3 and 1−5, respectively)

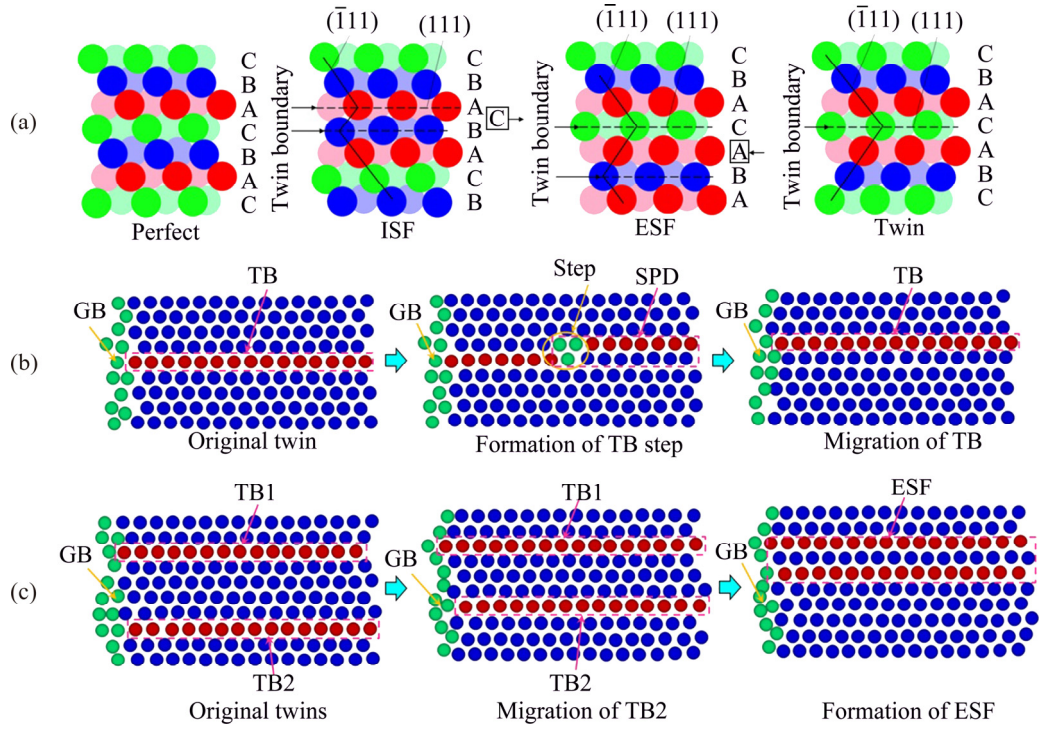

Fig. 11 Schematic illustrations for evolution of plane defects in nanotwinned polycrystalline copper with {111} texture: (a) Typical plane defects in FCC crystal; (b) Formation of step at TB and migration of TB; (c) Formation of ESF induced by TB migration

$$BC=\delta C+B\delta \quad (2)$$

or

$$B'C'=\delta'C'+B'\delta' \quad (3)$$

As a consequence, a pair of SPDs including the leading partial dislocation δC ($\delta'C'$) and the trailing partial dislocation $B\delta$ ($B'\delta'$) are emitted from the blocked site and then they slip on the TB plane. Because the ISF is characterized by two layers of HCP atoms and the TB is only composed of one layer of HCP atoms, the slip of SPDs on the TB planes results in the annihilation of the initial TBs and the emergence of new TBs adjacent to the initial ones. Therefore, the steps can be observed before the SPDs encounter the GBs, while only the migration of TBs is able to be seen when the SPDs intersect with the GBs, as illustrated in Fig. 11(b). If a TB is migrated near another one and there exists only one layer of FCC atoms between the two TBs, an extrinsic stacking fault (ESF) will be observed, as illustrated in Fig. 11(c). This kind of ESF has been observed in the model with the inclining angle of 45°, as shown in Fig. 3(d) and Fig. 6(a).

Figure 10(b) shows the schematic illustration for the dislocation nucleation and evolution in the model with the inclining angle of 45°, where δC is firstly initiated from the GB as the leading partial dislocation and $A\delta$ is subsequently emitted from the GB as the trailing partial dislocation. Meanwhile, a pair of SPDs including leading partial dislocation $\delta'C'$ and the trailing partial dislocation $A'\delta'$ are successively emitted from the GB. The above two pairs of SPDs slip in the matrix and the twin, respectively, until they intersect with the other side of the GB. If these SPDs are initiated at the junctions between the GBs and the TBs (as dislocations δC ($\delta'C'$) and $A\delta$ ($A'\delta'$) shown in Fig. 10(b)), the steps at TBs or the migration of TBs illustrated in Fig. 11(b) will be observed.

Figure 10(c) shows the schematic illustration for the dislocation nucleation, evolution and interaction in the model with the inclining angle of 90°, where a pair of SPDs including the leading partial dislocation βA and the trailing partial dislocation $D\beta$ is successively initiated from the GB. They slip in the matrix and are constricted into a full dislocation DA (as shown in Figs. 10(c_1, c_2)) when they encounter the TB. Subsequently, the dislocation DA is blocked by the TB and then the following dislocation dissociation

reaction occurs at the intersection site with increasing stress [1,2,17]:

$$DA=D\delta+\delta A\ \ (1/2[101]_{M}\rightarrow 1/6[1\bar{2}1]_{M}+1/3[111]_{M}) \quad (4)$$

After this reaction, the generated sessile Frank dislocation $D\delta$ is pinned at the TB while the glissile SPD δA slips at the TB (as shown in Fig. 10(c_3)), which results in the steps at the TB or the migration of TB illustrated in Fig. 11(b). The TB steps and the migration of TBs have been observed in experiment [52]. If the SPD δA encounters the pinned Frank dislocation $D\delta$ during the slipping, it will be blocked as well and the blocked site may become the source of a new SPD, as shown in Fig. 7(c). It has been confirmed by the experiments that steps at TBs are also the stress concentration sites and they can trigger the emission of dislocations as well [53,54]. The dissociation of dislocation is energetically unfavorable and requires a higher stress concentration to trigger it, so strengthening occurs in this case. With further proceeding of deformation, more and more dislocations are blocked at the intersection sites between the dislocations and the TBs, which results in such a much higher stress concentration at these sites that some hampered dislocations may pass through the TBs by means of the following reaction and participate in the dislocation emission in the twin [19,55]:

$$DA=C'D'+B'\delta'$$
$$(1/2[101]_{M}\rightarrow 1/2[0\bar{1}1]_{T}+1/6[\bar{1}\,\bar{1}2]_{T}) \quad (5)$$

By means of the above reaction, a dislocation $C'D'$ glides into the twin lamella and simultaneously the SPD $B'\delta'$ slips along the TB, which leads to the increase of step height and the further migration of the TB, as illustrated in Fig. 10(c_4), where the perfect dislocation $C'D'$ is emitted in the form of a pair of SPDs including the leading partial dislocation $\beta'D'$ and the trailing partial dislocation $C'\beta'$. With the further proceeding of deformation, the aforementioned dislocation reactions occur successively in the adjacent matrix and twin lamellae, which realizes the plastic deformation in the whole grain.

Based on the aforementioned analysis, it can be concluded that the occurrence of strengthening in the models with the inclining angles of 0° and 90° is associated with not only the Schmid factor but also the dislocation reaction induced by the dislocation block. In the case of 0°, only one kind of dislocation reaction is generated at the blocked sites, while two kinds of dislocation reactions occur in the case of 90°. In addition, the dislocation reactions in the case of 90° occur successively at each TB so that the plastic deformation is induced in the whole grain, which requires much higher stress to pass through each blocked site. As a consequence, the model with the inclining angle of 90° presents much more considerable strengthening behavior shown in Fig. 2.

It has been well known that there exist hard and soft orientations during the uniaxial deformation of anisotropic materials. The hard orientation can provide strengthening effect for the materials under uniaxial deformation, which results in higher yield stress of the materials. The soft orientation can bring soft effect to the materials under uniaxial deformation, which leads to the lower strength of materials. Based on the aforementioned results and analysis, the nanotwinned polycrystalline copper with {111} texture presents hardening behavior when the inclining angles of the TBs to the loading direction are 0° and 90°, while it exhibits soft behavior when the inclining angle is 45°. As a consequence, in the nanotwinned polycrystalline copper with {111} texture, the orientations with the inclining angles of 0° and 90° are the hard orientations and the orientation with the inclining angle of 45° is the soft one. The existence of hard and soft orientations is a key factor that leads to the plastic anisotropy of the nanotwinned polycrystalline copper with {111} texture.

On the basis of above simulated results and analysis, it is not denied that the dislocation behaviors and plastic mechanisms of nanotwinned polycrystalline copper with {111} texture vary with the angle between the loading direction and the TBs, i.e. the TB inclining angle, as summarized in Fig. 12. It can be seen that in the case of 0°, S1 slip system is dominant and the TB steps are induced by the SPDs resulting from a kind of dislocation reaction, which requires a higher stress. In the case of 45°, S2 slip system governs the plastic deformation and the TB steps come from the slip of this system. In the case of 90°, S3 slip system is dominating in the plastic deformation and the steps result from two kinds of dislocation reactions, which need much higher stress. In addition, the

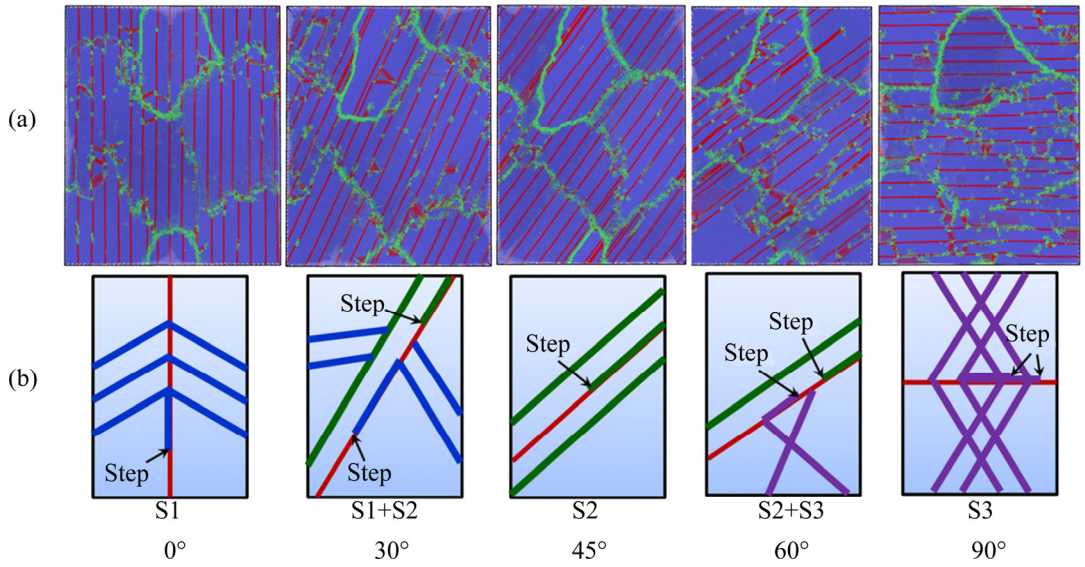

Fig. 12 General dislocation behaviors (a) and plastic mechanisms (b) of nanotwinned polycrystalline copper with {111} texture at TB inclining angles from 0° to 90° (In (b), the red lines represent the TBs, the blue lines stand for the SPDs induced by S1 slip system, the green lines denote the SPDs induced by the S2 slip system, and the purple lines describe the SPDs induced by S3 slip systems)

Schmid factor f_i (i=0, 45 and 90) of dominant slip systems in the three cases follow the sequence of $f_{45}>f_0>f_{90}$, as illustrated in Fig. 9. As a result, the case of 90° presents much higher level of yield stress and the case of 45° plays the lowest level of yield stress, while the yield stress in the case of 0° is between those of the above two cases, as shown in Fig. 2. This agrees with previous investigations on the columnar-nanotwinned copper with {111} texture, where the cases of 90° and 0° are regarded as the hard models and the case of 45° is treated as the soft model [31,33,56]. As for the case of 30°, both the characteristics of 0° and 45° models are observed from Fig. 12(a), so the plastic deformation in this case is operated by the combination of S1 and S2 slip systems. As for the case of 60°, the evolution behaviors present the characteristics of both 45° and 90° models, and thereby S2 and S3 slip systems cooperatively control the plastic deformation of this case. As a consequence, the yield stress of 30° model is between those of the 0° and 45° cases and yield stress of 60° model is between those of the 45° and 90° cases, which confirms the simulated results in Fig. 2.

5 Conclusions

(1) The nanotwinned polycrystalline copper with {111} texture presents obvious plastic anisotropy during tensile deformation. The mechanisms of this plastic anisotropy are revealed from the aspects of the Schmid factor of dominant slip system as well as dislocation mechanism based on MD simulation.

(2) The plastic anisotropy in the nanotwinned polycrystalline copper with {111} texture is closely related to the Schmid factor of dominated slip system, which is altered by changing the inclining angle of the TBs. However, the yield stress or the flow stress of the nanotwinned polycrystalline copper with {111} texture does not strictly follow the Schmid law, which indicates that the plastic anisotropy of nanotwinned polycrystalline copper with {111} texture is not influenced by the Schmid factor alone.

(3) In addition to the Schmid factor of dominant slip system, the plastic anisotropy in the nanotwinned polycrystalline copper with {111} texture is also aroused by the different dislocation mechanisms in the orientations with different TB inclining angles. In the nanotwinned polycrystalline copper with {111} texture, the orientations with the inclining angles of 0° and 90° are the hard orientations and the orientation with the inclining angle of 45° is the soft one. The strengthening mechanism of hard orientation in the nanotwinned

polycrystal copper with {111} texture lies in the fact that there exist interactions between the dislocations and the TBs during plastic deformation, which leads to the dislocation blocking and reactions. However, the softening mechanism of soft orientation in the nanotwinned polycrystal copper with {111} texture lies in the fact that there is no interaction between the dislocations and the TBs because only the slip systems parallel to the TBs are activated and the dislocations slip on the planes parallel to the TBs.

Acknowledgments

This work was supported by the National Natural Science Foundation of China (No. 51871070).

References

[1] LU L, SHEN Y F, CHEN X H, QIAN L H, LU K. Ultrahigh strength and high electrical conductivity in copper [J]. Science, 2004, 304: 422−426.

[2] MA E, WANG Y M, LU Q H, SUI M L, LU L, LU K. Strain hardening and large tensile elongation in ultrahigh-strength nano-twinned copper [J]. Applied Physics Letters, 2004, 85: 4932−4934.

[3] XIAO X Z, SONG D K, CHU H J, XUE J M, DUAN H L. Mechanical behaviors of irradiated FCC polycrystals with nanotwins [J]. International Journal of Plasticity, 2015, 74: 110−126.

[4] LU L, CHEN X, HUANG X, LU K. Revealing the maximum strength in nanotwinned copper [J]. Science, 2009, 323: 607−610.

[5] SCHIØTZ J, JACOBSEN K W. A maximum in the strength of nanocrystalline copper [J]. Science, 2003, 301: 1357−1359.

[6] MAHAJAN S, BARRY D E, EYRE B L. A thin twin and its interaction with a coherent twin boundary in copper [J]. Philosophical Magazine, 1970, 21: 43−52.

[7] LU K, LU L, SURESH S. Strengthening materials by engineering coherent internal boundaries at the nanoscale [J]. Science, 2009, 324: 349−352.

[8] YANG X S, ZHAI H R, RUAN H H, SHI S Q, ZHANG T Y. Multi-temperature indentation creep tests on nanotwinned copper [J]. International Journal of Plasticity, 2018, 104: 68−79.

[9] TUCKER G J, FOILES S M. Quantifying the influence of twin boundaries on the deformation of nanocrystalline copper using atomistic simulations [J]. International Journal of Plasticity, 2015, 65: 191−205.

[10] WANG J W, SANSOZ F, HUANG J Y, LIU Y, SUN S H, ZHANG Z, MAO S X. Near-ideal theoretical strength in gold nanowires containing angstrom scale twins [J]. Nature Communication, 2013, 4: 1−8.

[11] LI X Y, WEI Y J, LU L, LU K, GAO H J. Dislocation nucleation governed softening and maximum strength in nano-twinned metals [J]. Nature, 2010, 464: 877−880.

[12] WU L P, YU W S, HU S L, SHEN S P. Stability of stacking fault tetrahedron in twin boundary bicrystal copper under shear [J]. International Journal of Plasticity, 2017, 97: 246−258.

[13] TANG Xiao-zhi, ZHANG Hui-shi, GUO Ya-fang. Atomistic simulations of interactions between screw dislocation and twin boundaries in zirconium [J]. Transactions of Nonferrous Metals Society of China, 2018, 28: 1192−1199.

[14] WU Hai-chen, YU You-xing, BI Xiao-fang. Atomic scale structural characterization of {1012} twin boundaries in zinc [J]. Transactions of Nonferrous Metals Society of China, 2018, 28: 1538−1542.

[15] GUO Li-li, FUJITA F. Effect of deformation mode, dynamic recrystallization and twinning on rolling texture evolution of AZ31 magnesium alloys [J]. Transactions of Nonferrous Metals Society of China, 2018, 28: 1094−1102.

[16] JIN Z H, GUMBSCH P, MA E, ALBE K, LU K, HAHN H, GLEITER H. The interaction mechanism of screw dislocations with coherent twin boundaries in different face-centred cubic metals [J]. Scripta Materialia, 2006, 54: 1163−1168.

[17] WANG Y B, WU B, SUI M L. Dynamical dislocation emission processes from twin boundaries [J]. Applied Physics Letters, 2008, 93: 041906.

[18] WU Z X, ZHANG Y W, SROLOVITA D J. Dislocation–twin interaction mechanisms for ultrahigh strength and ductility in nanotwinned metals [J]. Acta Matererialia, 2009, 57: 4508−4518.

[19] JIN Z H, GUMBSCH P, ALBE K, MA E, LU K, GLEITER H, HAHN H. Interactions between non-screw lattice dislocations and coherent twin boundaries in face-centered cubic metals [J]. Acta Materialia, 2008, 56: 1126−1135.

[20] ANDEROGLU O, MISRA A, WANG J, HOAGLAND R G, HIRTH J P, ZHANG X. Plastic flow stability of nanotwinned Cu foils [J]. International Journal of Plasticity, 2010, 26: 875−886.

[21] LU L, YOU Z S, LU K. Work hardening of polycrystalline Cu with nanoscale twins [J]. Scripta Materialia, 2012, 66: 837−842.

[22] CHEN X H, LU L, LU K. Grain size dependence of tensile properties in ultrafine-grained Cu with nanoscale twins [J]. Scripta Materialia, 2011, 64: 311−314.

[23] MISRA A, HIRTH J P, HOAGLAND R G. Length-scale-dependent deformation mechanisms in incoherent metallic multilayered composites [J]. Acta Materialia, 2005, 53: 4817−4824.

[24] WU Z X, ZHANG Y W, SROLOVITZ D J. Deformation mechanisms, length scales and optimizing the mechanical properties of nanotwinned metals [J]. Acta Materialia, 2011, 59: 6890−6900.

[25] LU L, SCHWAIGER R, SHAN Z W, DAO M, LU K, SURESH S. Nano-sized twins induce high rate sensitivity of flow stress in pure copper [J]. Acta Materialia, 2005, 53: 2169−2179.

[26] DAO M, LU L, SHEN Y F, SURESH S. Strength, strain-rate sensitivity and ductility of copper with nanoscale twins [J].

Acta Materialia, 2006, 54: 5421−5432.
[27] SHEN Y F, LU L, DAO M, SURESH S. Strain rate sensitivity of Cu with nanoscale twins [J]. Scripta Materialia, 2006, 55: 319−322.
[28] SHABIB I, MILLER R E. A molecular dynamics study of twin width, grain size and temperature effects on the toughness of 2D-columnar nanotwinned copper [J]. Modelling and Simulation in Materials Science and Engineering, 2009, 17: 055009.
[29] CHENG Z, ZHOU H F, LU Q H, GAO H J, LU L. Extra strengthening and work hardening in gradient nanotwinned metals [J]. Science, 2018, 362: 559.
[30] YOU Z S, LU L, LU K. Tensile behavior of columnar grained Cu with preferentially oriented nanoscale twins [J]. Acta Materialia, 2011, 59: 6927−6937.
[31] JANG D C, LI X Y, GAO H J, GREER J R. Deformation mechanisms in nanotwinned metal nanopillars [J]. Nature Nanotechnology, 2012, 7: 594−601.
[32] ZHAO X, LU C, TIEU A K, ZHAN L H, HUANG M H, SU L H, PEI L Q, ZHANG L. Deformation twinning and dislocation processes in nanotwinned copper by molecular dynamics simulations [J]. Computational Materials Science, 2018, 142: 59−71.
[33] YOU Z S, LI X Y, GUI L J, LU Q H, ZHU T, GAO H J, LU L. Plastic anisotropy and associated deformation mechanisms in nanotwinned metals [J]. Acta Materialia, 2013, 61: 217−227.
[34] HUANG S, BEYERLEIN I J, ZHOU C. Unusual size effects from tilted twin boundaries in nano-twinned metals [J]. Extreme Mechanics Letters, 2019, 32: 100571.
[35] LAGRANGE T, REED B W, WALL M, MASON J, BARBEE T, KUMAR M. Topological view of the thermal stability of nanotwinned copper [J]. Applied Physics Letters, 2013, 102: 011905.
[36] MURR L E. Strain-induced dislocation emission from grain boundaries in stainless steel [J]. Materials Science and Engineering A, 1981, 51: 71−79.
[37] SHIMOKAWA T. Asymmetric ability of grain boundaries to generate dislocations under tensile or compressive loadings [J]. Physical Review B, 2010, 82: 174122.
[38] YUASA M, NAKAZAWA T, MABUCHI M. Atomic simulations of dislocation emission from Cu/Cu and Co/Cu grain boundaries [J]. Materials Science and Engineering A, 2010, 528: 260−267.
[39] FRØSETH A G, van SWYGENHOVEN H, DERLET P M. Developing realistic grain boundary networks for use in molecular dynamics simulations [J]. Acta Materialia, 2005, 53: 4847−4856.
[40] MISHIN Y, MEHL M J, PAPACONSTANTOPOULOS D A, VOTER A F, KRESS J D. Structural stability and lattice defects in copper: Ab initio, tight-binding, and embedded-atom calculations [J]. Physics Review B, 2001, 63: 224106.
[41] ZHAO X, LU C, TIEU A K, PEI L Q, ZHANG L, CHENG K Y, HUANG M H. Strengthening mechanisms and dislocation processes in ⟨111⟩ textured nanotwinned copper [J]. Materials Science and Engineering A, 2016, 676: 474−486.
[42] PLIMPTON S. Fast parallel algorithms for short-range molecular dynamics [J]. Journal of Computational Physics, 1995, 117: 1−19.
[43] ZHANG J X, GHOSH S. Molecular dynamics based study and characterization of deformation mechanisms near a crack in a crystalline material [J]. Journal of Mechanics and Physics of Solids, 2013, 61: 1670−1690.
[44] STUKOWSKI A. Visualization and analysis of atomistic simulation data with OVITO–The open visualization tool [J]. Modelling and Simulation in Materials Science and Engineering, 2010, 18: 015012.
[45] STANFORD N, SOTOUDEH K, BATE P S. Deformation mechanisms and plastic anisotropy in magnesium alloy AZ31 [J]. Acta Materialia, 2011, 59: 4866−4874.
[46] LI L L, ZHANG Z J, ZHANG P, WANG Z G, ZHANG Z F. Controllable fatigue cracking mechanisms of copper bicrystals with a coherent twin boundary [J]. Nature Communication, 2014, 5: 3536.
[47] WRONSKI S, WROBEL M, BACZMANSKI A, WIERZBANOWSKI K. Effects of cross-rolling on residual stress, texture and plastic anisotropy in f.c.c. and b.c.c. metals [J]. Materials Characterization, 2013, 77: 116−126.
[48] ZHANG Z F, WANG Z G. Grain boundary effects on cyclic deformation and fatigue damage [J]. Progress in Materials Science, 2008, 53: 1025−1099.
[49] KRASNIKOV V S, MAYER A E. Plasticity driven growth of nanovoids and strength of aluminum at high rate tension: Molecular dynamics simulations and continuum modeling [J]. International Journal of Plasticity, 2015, 74: 75−91.
[50] ZHANG Y Q, JIANG S Y. Investigation on dislocation-based mechanisms of void growth and coalescence in single crystal and nanotwinned nickels by molecular dynamics simulation [J]. Philosophical Magazine, 2017, 97: 2772−2794.
[51] SAINATH G, CHOUDHARY B K. Molecular dynamics simulation of twin boundary effect on deformation of Cu nanopillars [J]. Physics Letters A, 2015, 379: 1902−1905.
[52] WANG Y B, SUI M L, MA E. In situ observation of twin boundary migration in copper with nanoscale twins during tensile deformation [J]. Philosophical Magazine Letters, 2007, 87: 935−942.
[53] SENNOUR M, LARTIGUE-KORINEK S, CHAMPION Y, HYTCH M J. HRTEM study of defects in twin boundaries of ultra-fine grained copper [J]. Philosophical Magazine, 2007, 87: 1465−1486.
[54] KONOPKA K, MIZERA J, WYRZYKOWSKI J W. The generation of dislocations from twin boundaries and its effect upon the flow stresses in FCC metals [J]. Journal of Materials Processing Technology, 2000, 99: 255−259.
[55] ZHANG X, MISRA A, WANG H, NASTASI M, EMBURY J D, MITCHELL T E, HOAGLAND R G, HIRTH J P. Nanoscale-twinning-induced strengthening in austenitic stainless steel thin films [J]. Applied Physics Letters, 2004, 84: 1096−1098.
[56] ZHU T, GAO H J. Plastic deformation mechanism in nanotwinned metals: An insight from molecular dynamics and mechanistic modeling [J]. Scripta Materialia, 2012, 66: 843−848.

含有{111}织构的纳米孪晶多晶铜在拉伸变形过程中塑性各向异性机制的分子动力学模拟

张艳秋，江树勇

哈尔滨工程大学 机电工程学院，哈尔滨 150001

摘　要：基于分子动力学模拟，从主导滑移系的斯密特因子和位错机制两个方面系统研究含有{111}织构的纳米孪晶多晶铜在拉伸变形过程中的塑性各向异性机制。结果表明：主导滑移系的斯密特因子随着孪晶界倾角的改变而变化，但屈服应力或流动应力并不严格遵守斯密特定律。在拉伸变形过程中存在涉及不同位错机制的硬取向和软取向。硬取向的硬化机制在于塑性变形过程中存在位错与孪晶界之间的相互作用，从而导致位错塞积和位错反应。软取向的软化机制在于没有位错与孪晶界之间的相互作用，这是由于只有平行于孪晶界的滑移系被激活，使得位错在平行于孪晶界的晶面上运动。因此，可以推断，含有{111}织构的纳米孪晶多晶铜的塑性各向异性是由主导滑移系的斯密特因子与位错机制共同作用的结果。

关键词：力学性能；位错；分子动力学；塑性各向异性；纳米孪晶

(Edited by Bing YANG)